Specific luminescence studies in plastic scintillators*

L. Muga and G. Griffith
Chemistry Department, University of Florida, Gainesville, Florida 32601
(Received 9 October 1973)

Using a thin-film scintillator detector direct measurements of relative specific luminescence ($\Delta L / \Delta x$) and luminescence efficiency ($\Delta L / \Delta E$) values have been obtained for an organic scintillator exposed to transiting light and heavy ions. These experimentally obtained luminescence data are presented as a function of ion energy, velocity, and stopping power for a wide variety of transiting ions ($Z = 1,2,8,17,18,35,53$). The data emphasize the luminescence response in the low-energy range corresponding to maximum ion stopping power. Common trends, unique characteristics, and other interesting features pertinent to these graphical plots are noted and discussed. The double-valuedness of the specific luminescence $\Delta L / \Delta x$ when plotted as a function of specific energy loss $\Delta E / \Delta x$ is interpreted as arising mainly from the decreased effective charge of the ion as it picks up electrons in the slowing-down process. It is further emphasized that the specific energy-loss *per se* is an inappropriate parameter for characterizing (in a direct way) the luminescence response. A new model is formulated based on a conceptually different approach to the problem of luminescence production along and about the path of a transiting energetic ion. In essence, the number of electrons scattered into a thin disk of scintillator material (perpendicular to the ion trajectory) is taken, in the absence of saturation effects, as proportional to the luminescence response from that disk. Saturation effects are included by deriving an explicit relation for the number of electrons scattered per unit area of disk at a distance r from the ion path. Above a critical number per unit area, no additional luminescence response is generated. These number-density profiles are plotted for various ions of different energies. Finally, a plot of the calculated specific luminescence for various heavy ions is shown to be in remarkably good agreement with experimental data.

I. INTRODUCTION

The dependence of specific luminescence ($\Delta L/\Delta x$) and luminescence efficiency ($\Delta L/\Delta E$) upon stopping power (dE/dx) of heavy ionizing particles (impinging on fluorescent materials) has been the subject of intensive study.[1-8] Although a wide range of energies has been considered, comparatively little effort has been made toward observing and understanding the specific-luminescence response in the low-energy region corresponding to maximum stopping power. This lack of completeness is in large measure the result of serious difficulties in experimental observation of luminescence ΔL when the incident heavy ionizing particle has large dE/dx values (i.e., at low velocities). The major experimental work and theoretical discussion (model formulation) has been made with regards to inorganic scintillator detectors [e.g., NaI (Tl)]. The usual approach is to unfold the differential luminescence response (dL/dx and dL/dE) from integral response curves (L vs E) for which the ionizing particle (of known energy) is completely stopped in the fluorescent material. At very low velocities (and high dE/dx values), this unfolding leads to large uncertainties. On the other hand, to measure the specific luminescence dL/dx directly requires ultrathin fluorescent materials coupled with an efficient light collecting system. Such a system has recently become available[9] and uses thin films of plastic scintillators (e.g., NE-102) of a thickness several orders of magnitude smaller than the thinnest inorganic scintillator detectors previously used. Thus, specific luminescence may be directly recorded for individual heavy ionizing particles.

Although the mechanism of light production and collection in plastic versus inorganic scintillators is popularly regarded as quite different, sufficient resemblence in over-all luminescence response does exist (and has been observed) such that a limited comparison is justified. Organic-scintillator materials have the additional benefit of being more nearly tissue like in their composition (as opposed to inorganic scintillators) and their study may lead to deeper insight into the mechanisms of linear energy transfer (LET) of heavy ionizing particles in living tissue, a subject of much current interest.

The goal of this paper is to review the work to date using thin-film scintillator detectors as a tool for direct specific-luminescence determinations of ionizing nuclear particles and to compare the results with those predicted from models previously formulated regarding light production and collection in scintillator materials. Finally, a new model for luminescence response is developed that is based on a conceptually different approach from other reported models.

II. EXPERIMENTAL

The general scheme of the experiment is diagrammed in Fig. 1. Incident ions passed through

Copyright © 1974 by The American Physical Society.

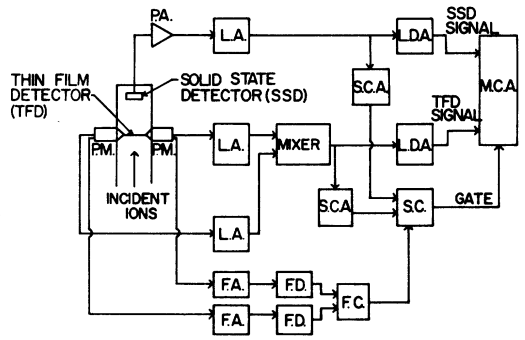

P.M.	PHOTOMULTIPLIER	S.C.	SLOW COINC.
P.A.	PREAMP.	F.C.	FAST COINC.
L.A.	LINEAR AMP.	F.A.	FAST AMP.
S.C.A.	SINGLE CHAN. ANALYZER	F.D.	FAST DISC.
L.D.A.	LINEAR DELAY AMP.	M.C.A.	MULTICHANNEL ANALYZER

FIG. 1. Diagram of experimental approach for measuring specific luminescence of thin plastic scintillator.

a thin-film detector (TFD) and entered a solid state detector (SSD) positioned behind it. Signals from the SSD were used both to gate the counting system and to measure the residual energy of the individual transiting ion. Incident ion energies were measured by placing the SSD in front of the TFD, thus intercepting the ion beam prior to its passage through the TFD. Calibration of the SSD with known-energy α particles or heavy ions allowed an experimental determination to be made of energy loss in the thin-film detector at each ion energy. Frequent referencing of the TFD response was made by exposing it to a radioactive source emitting monoenergetic α particles and/or to a ^{252}Cf spontaneously fissioning source in order to eliminate the problem of pulse-height amplitude-gain drift and to cross reference incident-ion response curves taken under different conditions.

Energetic ion sources were employed as follows.

(a) Light ions ($Z = 1, 2$): Protons, deuterons, ^{3}He, and ^{4}He ions, accelerated with the University of Florida 4-MeV Van de Graaff, were elastically scattered from a thin (0.1 mg/cm^2) nickel target and then collimated to impinge on the central portion of the TFD-SSD system.[10]

(b) Intermediate ions ($Z = 8$): ^{16}O ions, accelerated at the Florida State University tandem Van de Graaff facility, were allowed to scatter from a thin (0.1 mg/cm^2) nickel foil at selected angles to achieve a wide choice of energies of ions incident on the TFD-SSD assembly.[11]

(c) Heavy ions ($Z = 8, 17, 18, 35, 53$): Using multicomponent and/or monoenergetic beams selected by calibrated bending magnets, known energy groups of heavy ions were accelerated at the ORNL tandem Van de Graaff.[12] The ion beams were attenuated in intensity such that they were allowed to impinge directly on the TFD-SSD system.

The thin-film detectors were fabricated according to previously reported procedures[9] and different numbers of laminations of thin scintillator films were used to establish the effect of thickness on specific-luminescence response. The plastic scintillator[13] most often used was NE-102 although, on occasion, the response of a faster decay scintillator, NE-111, was studied. A drawing of the thin-film detector is shown in Fig. 2.

The solid-state detectors used were of the surface-barrier type available from ORTEC, Inc., and were chosen such that the sensitive depth always exceeded the maximum range of the ions under study.

It is important to recognize that relative specific-luminescence $\Delta L/\Delta x$ values were measured *directly* in these experiments as a function of the known particle incident and residual energy.

III. RESULTS AND DISCUSSION

A. Summary of experimental data

In unfolding the energetic ion ($Z \geq 1$) luminescence response of inorganic scintillators from integral-luminescence–vs–ion-energy curves, it is customary to plot the luminescence efficiency $\Delta L/\Delta E$ against those parameters of interest. The rational for these plots is based on the intuitive feeling that the luminescence per unit ion-path length should be normalized to the corresponding ion energy loss, i.e., in order to reduce the response of

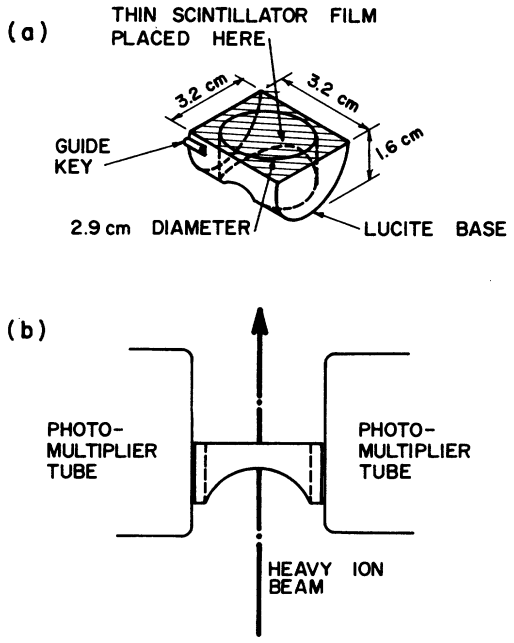

FIG. 2. Drawing of thin-film scintillator detector used for measuring luminescence caused by energetic light and heavy ions transiting thin plastic scintillator.

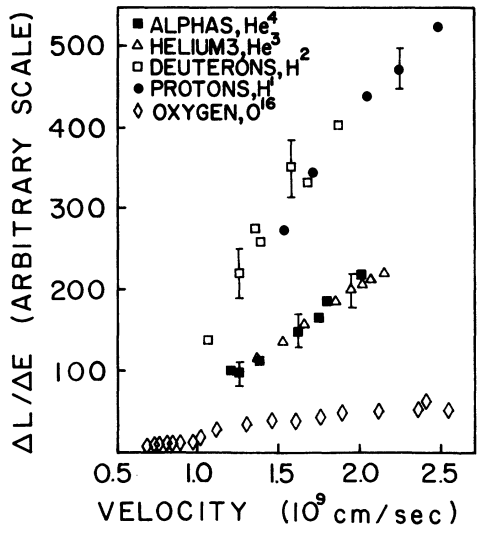

FIG. 3. Luminescence efficiency $\Delta L/\Delta E$ vs ion velocity for transiting light ions. Scintillator material is NE-102 for this and following figures unless otherwise stated.

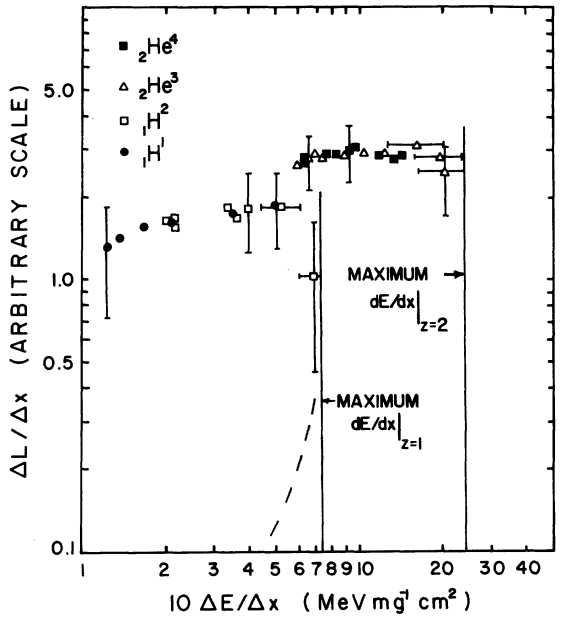

FIG. 5. Specific luminescence $\Delta L/\Delta x$ vs specific energy loss $\Delta E/\Delta x$ for incident light ions.

different particles to a common denominator. This concept implies that specific energy loss dE/dx is a suitably appropriate parameter for understanding the luminescence process. Following this trend, Figs. 3 and 4 present luminescence efficiency as a function of ion velocity for transiting light ($Z = 1$, 2, 8) and heavy ions ($Z = 8$, 17, 18, 35, 53), respectively. We note that in the case of NE-102 plastic scintillator, for a given velocity, the lighter ion is more efficient in photon production and this response parallels observations previously reported for inorganic scintillators.[14] Furthermore, the efficiency is relatively independent of ion mass (compare protons with deuterons and ^{3}He with ^{4}He), but clearly has a strong charge dependence. At higher velocities the luminescence efficiency tends to level off to a constant value for a given ion. At lower velocities (and low energies) the efficiencies of all ions tend to converge and are more closely grouped.

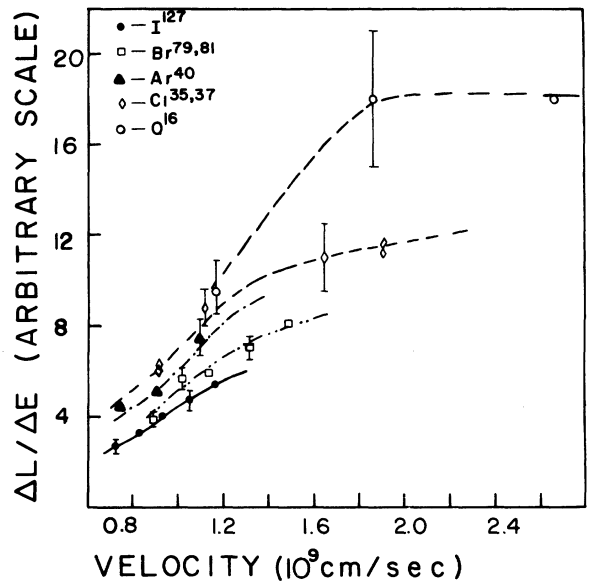

FIG. 4. Luminescence efficiency $\Delta L/\Delta E$ vs ion velocity for transiting heavy ions; curved lines are added as visual aid. The ordinate scale (arbitrary) is different from that of Fig. 3, but may be compared through the ^{16}O-ion response, which is common to both figures.

In particular, we do not observe the upswing in efficiency at energies below those corresponding to maximum ion stopping power as predicted by the calculations of Murray and Myer[14] and as reportedly observed by Allison and Casson[3] for α particles penetrating NaI(Tl) crystals. We should emphasize, however, that the two systems, viz, organic vs inorganic scintillators, are different and direct comparison may not be in order. We are in qualitative agreement with the NaI(Tl) data of Altman *et al.* as reported by Luntz and Heymsfield.[15]

The experimental relationship between differential luminescence ΔL and energy loss ΔE is shown in Figs. 5–7 for which specific luminescence $\Delta L/\Delta x$ (proportional to TFD response) vs specific energy loss or stopping power, $\Delta E/\Delta x$, is plotted. In Fig. 5, transiting-light-ion ($Z = 1$, 2) data indicate a linear response at low dE/dx and high velocity and energy tending to a maximum value followed

by a precipitous drop in specific luminescence just before the maximum dE/dx value is reached. On the other hand, the available data for heavy ions (excepting ^{16}O) (Fig. 6) show an increasingly larger luminescence response as dE/dx approaches (but from lower velocity) maximum values. The connection between the two sets of data (Figs. 5 and 6) is evident in the more comprehensive data shown in Fig. 7 for transiting ^{16}O ions in NE-111 plastic scintillator. Here, the specific-luminescence response is shown for a range of energies which bracket that corresponding to maximum dE/dx value. A similar response (with much more detail) was obtained for ^{16}O ions penetrating NE-102 plastic-scintillator films and is shown in Fig. 2 of Ref. 11. The precipitous drop in specific luminescence (as ion energy decreases) occurs just before but not coincident with that corresponding to maximum dE/dx values and is similar to that reported for NaI(Tl).[5]

The form of this precipitous drop (as ion energies are reduced to the range of maximum stopping power) is akin to that predicted by the model of Katz and Kobetich.[16] The values of stopping power at which an abrupt decrease in specific luminescence occurs, although different in absolute magnitude, are comparable when compared relative to the maximum value of dE/dx in NaI(Tl) and NE-102 materials, ~3.4 and ~18 MeV/mg cm^{-2}, respectively.[17] In its approach to maximum stopping-power values, the $\Delta L/\Delta x$-vs-$\Delta E/\Delta x$ curve as observed by us is distinct both in shape and absolute

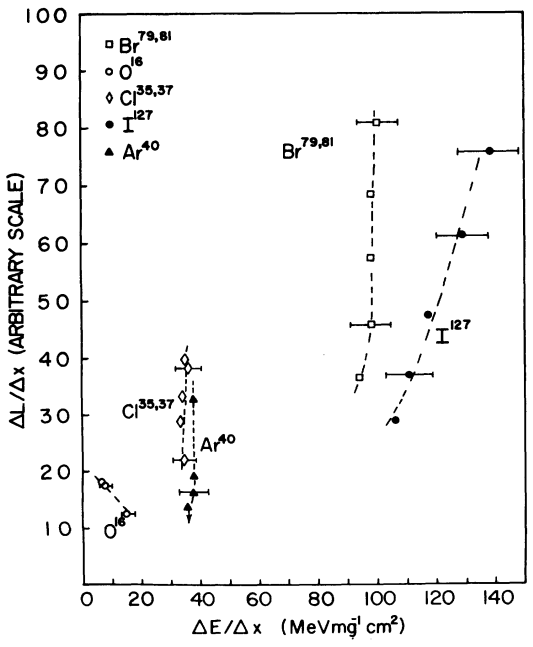

FIG. 6. Specific luminescence $\Delta L/\Delta x$ vs specific energy-loss $\Delta E/\Delta x$ for incident heavy ions.

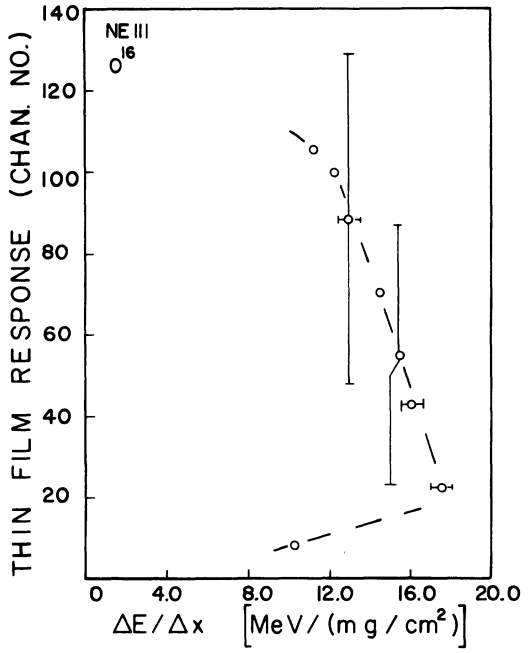

FIG. 7. Thin-film response to passing ^{16}O ions plotted as a function of specific energy loss. Scintillator is NE-111.

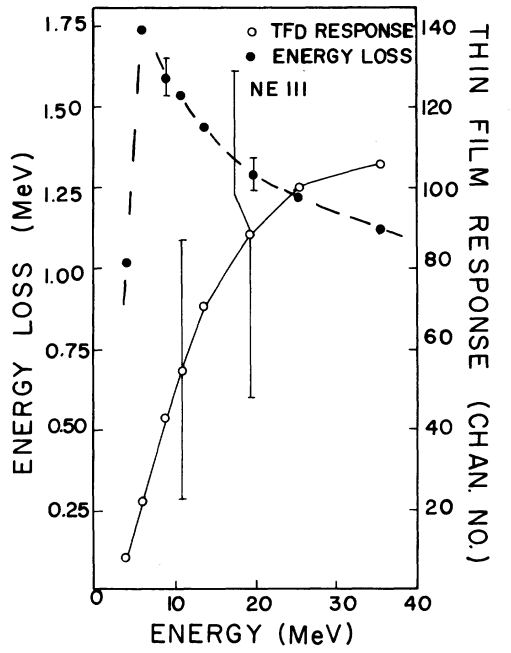

FIG. 8. Dependence of ion energy loss (solid circles) and thin-film response (open circles) on incident energy of transiting ^{16}O ions. Error bars on energy-loss data represent estimated statistical and systematic uncertainties. Limit bars on thin-film response represent the full width at half-maximum in the pulse-height distribution; the data points indicate the peak position. Scintillator is NE-111.

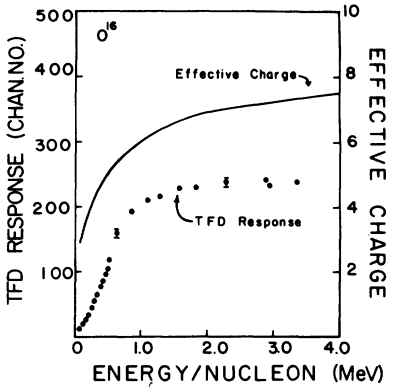

FIG. 9. Effective-ion charge (Ref. 18) (solid curve) and thin-film detector response ($\Delta L/\Delta x$) plotted against energy per nucleon of incident ^{16}O particle in NE-102.

magnitude from the calculated and experimentally observed response reported by others.[6,14] Our data are in agreement with the more recent results of da Silva and Voltz[8] for light and heavy ions ($Z = 1, 2, 7$) over the limited energy range for which matching data are reported.

The manner in which the specific energy loss relates to the specific luminescence is more clearly shown in Fig. 8 (and in Fig. 1 of Ref. 11), wherein dual plots of experimental data for specific luminescence and specific energy loss vs ion velocity are shown for the case of NE-111 plastic scintillator.

The double valuedness or "loop" dependence (see Fig. 7, and Fig. 2 of Ref. 11) of specific luminescence $\Delta L/\Delta x$ on specific energy loss $\Delta E/\Delta x$ is a consequence mainly of the decreased effective charge of the transiting ion as it picks up electrons in slowing down. This cause is clearly suggested by the plot of Fig. 9 for which the effective heavy-ion charge[18] is superimposed on the specific-luminescence-vs-energy-per-nucleon plot. The abrupt decrease in effective ion charge clearly coincides with the decreased luminescence yields at lower energies. Thus it would appear that specific energy loss is an inappropriate parameter for characterizing in simple terms the specific-luminescence response. It is further apparent that the ion velocity and effective ion charge (the latter being velocity dependent) are the elementary variables affecting this response. To complete this

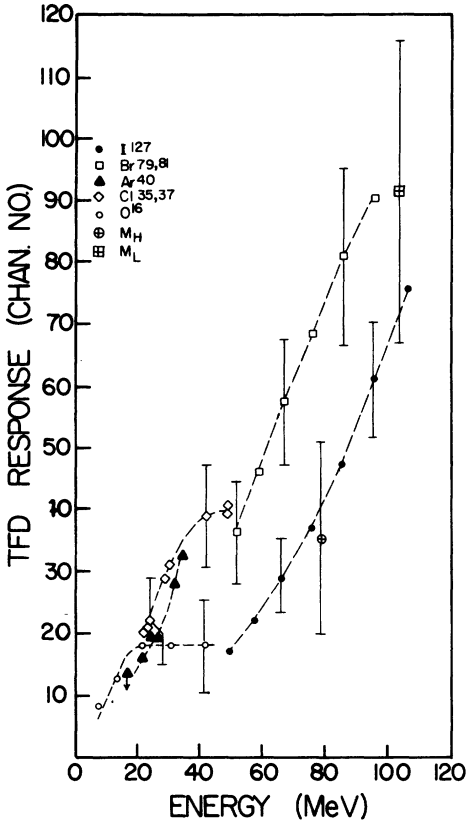

FIG. 11. Specific luminescence (TFD response) vs incident energy for various heavy ions transiting NE-102 scintillator film of 0.1-mg/cm^2 thickness. M_L and M_H refer to typical light and heavy fragments, respectively, from ^{252}Cf fission decay.

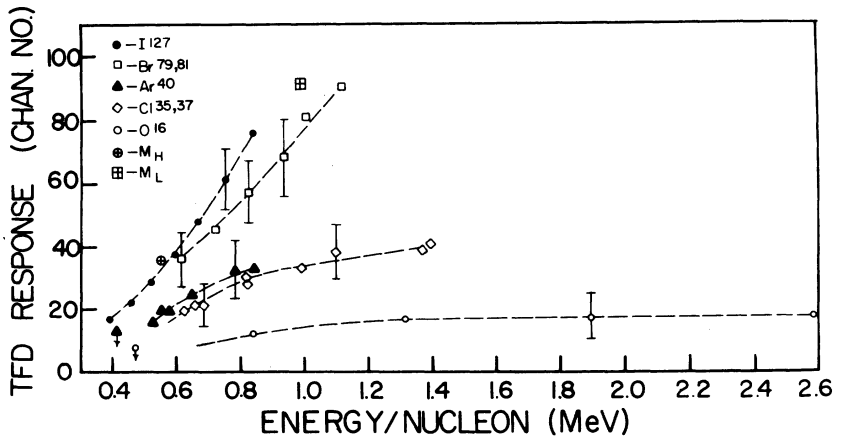

FIG. 10. Specific luminescence (TFD response) vs incident energy per nucleon for various heavy ions transiting NE-102 scintillator film of 0.1-mg/cm^2 thickness. M_L and M_H refer to typical light and heavy fragments, respectively, from ^{252}Cf fission decay.

section the family of curves depicting the specific-luminescence dependence on velocity and energy for various heavy ions penetrating NE-102 plastic scintillator is shown in Figs. 10 and 11, respectively.

B. Model for specific luminescence

Explanations of the nonlinear dependence of specific luminescence on specific energy loss may be placed in two categories. In the first, semiempirical relations are developed in terms of saturation or quenching mechanisms which reduce the luminescence efficiency at large values of the ion specific energy loss. In the second approach, the more fundamental relation between luminescence and velocity is attempted on the basis of an energy-deposition profile radially outward from the ion-trajectory axis. The underlying principle is the same in that luminescence is linked to ion energy loss; the latter approach is more refined in its treatment of the details of energy loss along the ion's path.

All of these recent formulations[15,19–21] are dependent upon some assumed function for describing the energy-deposition profile and also involve varying amounts of "curve fitting" or "parametrization" in the final analysis. We develop in this section a model which hopefully circumvents some of these shortcomings. As with previous models, we accept the position that the transiting heavy ion produces luminescence through the agency of scattered electrons, i.e., the direct interaction of the heavy ion is negligible. This description has been referred to as the "bristle-brush" picture, for which the wire core represents the undeviated heavy-ion trajectory and the bristles depict the paths of electrons scattered radially outward and in the forward direction. In order to quantitatively describe the luminescence response, we next develop a conceptually different approach after the manner of nuclear chemists for dealing with thin-target bombardments.[22] The cross section for a particular process is defined by the equation

$$L = In\sigma x \,, \tag{1}$$

where L is the number of processes of the type under consideration occurring in the target, I is the number of incident particles (scattered electrons in our case), n is the number of target nuclei (number of scintillator sites) per cubic centimeter of target, $\sigma(E)$ is the cross section for the specified process, generally dependent on energy of the incident particle and expressed in square centimeters, and x is the target thickness in centimeters. Briefly, our approach is to calculate the number of electrons scattered through a thin annular disk whose plane is perpendicular to the heavy-ion trajectory. Assuming a constant cross section $\sigma(E)$, and in the absence of saturation effects, this number is taken as proportional to luminescence. Saturation effects and effective-ion charge are next incorporated into the model to produce an expression for specific luminescence. A detailed derivation follows.

1. Electron scattering cross section

For the relatively low velocity range of heavy ions of interest we choose the classical Rutherford scattering formula[23] to describe the differential cross section σ_{sc} for scattering (or recoiling) of free electrons into the laboratory angle ϕ with respect to the heavy-ion direction, viz.,

$$\frac{d\sigma_{sc}}{d\phi} = -\tfrac{1}{2}\pi b^2 \tan\phi \sec^2\phi \,, \tag{2}$$

where

$$b = CZ_1Z_2e^2(M_1+M_2)/M_2E_1 \,. \tag{3}$$

Here, subscripts 1 and 2 refer, respectively, to transiting heavy ion and scattered (or recoiled) electron. Z, M, and E refer to charge number, mass (amu) and energy (MeV), respectively; e is the unit charge (esu) and C is a conversion factor (MeV/erg); b is expressed in centimeters.

From Eq. (2), the cross section for scattering of the electron between angles ϕ_n and ϕ_x is derived as

$$\sigma_{sc} = \tfrac{1}{4}\pi b^2(\tan^2\phi_n - \tan^2\phi_x) \,. \tag{4}$$

2. Energy and range of scattered electrons

The energy of the scattered electrons is given[23] approximately (assuming $M_2 \ll M_1$) as

$$E_2 = 4E_1(M_2/M_1)\cos^2\phi \,. \tag{5}$$

We take for the electron range R the low-energy form of the relation given by Weber[24] for aluminum, as reported by Kobetich and Katz,[20] viz.,

$$R = kE_2 \,, \tag{6}$$

where k is given as 9.93×10^{-3} g/cm^2 MeV. Dividing by the density of NE-102 (1.032 g/cm^3) we have $k = 9.62\times10^{-3}$ cm/MeV, with range R in centimeters.

Combining Eqs. (5) and (6) we arrive at the range relation

$$R = F\cos^2\phi \,, \tag{7}$$

$$\text{with } F = 4kE_1(M_2/M_1). \tag{8}$$

3. Number of incident electrons

Consider the number of electrons scattered at a distance x from a thin circular disk placed perpendicular to the path of the heavy ion as diagrammed in Fig. 12. Further, consider only those scattered electrons having mean ranges (and tra-

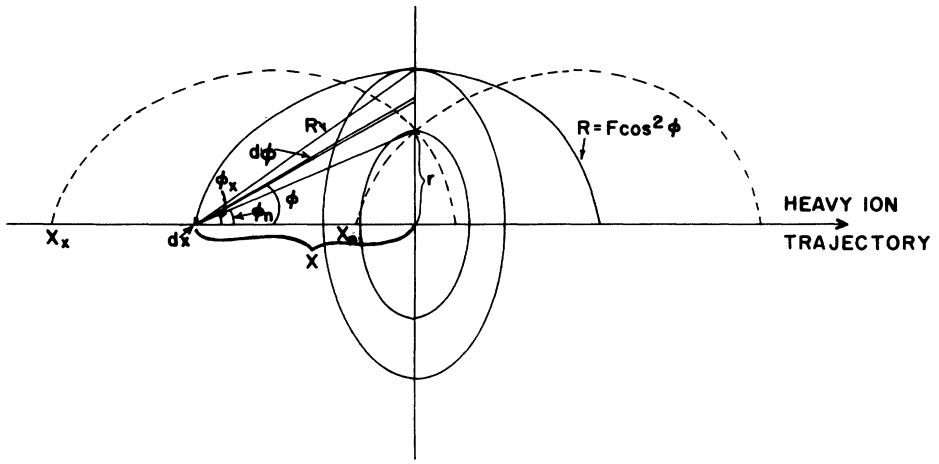

FIG. 12. Diagram depicting parameters for describing scattered electron into disk and at a distance r or greater from heavy-ion trajectory axis.

jectories) such that they pass through the disk at radius r or greater, corresponding to a scatter (or recoil) angle greater than ϕ_n. From the point at which scattering occurs (at distance x from the plane of the disk), the maximum scatter angle for which electrons will have sufficient range R to still penetrate the disk is ϕ_x. We neglect any change in direction due to secondary scattering of the electron from its original path.

The differential cross section (per heavy-ion path length) for electrons penetrating the disk at points outside radius r and originating from heavy-ion path length dx at distance x is

$$\frac{d\Sigma}{dx} = \int_{\phi_n}^{\phi_x} d\sigma_{sc} = \tfrac{1}{4}\pi b^2[\tan^2\phi_n - \tan^2\phi_x] , \tag{9}$$

for which

$$\phi_n = \arctan(r/x) , \tag{10}$$

and, making use of Eq. (7),

$$\phi_x = \arccos[(x/F)^{1/3}] . \tag{11}$$

Thus Eq. (9) reduces to

$$\frac{d\Sigma}{dx} = \tfrac{1}{4}\pi b^2\left[1 + \frac{r^2}{x^2} - \left(\frac{F}{x}\right)^{2/3}\right] . \tag{12}$$

Integrating Eq. (12) between the limits of x for which electrons may pass through the disk at radius greater than r gives the "volume" cross section for scattering,

$$\begin{aligned}\Sigma_{sc} &= \int_{x_x}^{x_n} \tfrac{1}{4}\pi b^2\left[1 + \frac{r^2}{x^2} - \left(\frac{F}{x}\right)^{2/3}\right] dx \\ &= \tfrac{1}{4}\pi b^2\left\{r^2\left(\frac{1}{x_x} - \frac{1}{x_n}\right) + F\left[\frac{x_n}{F} - \frac{x_x}{F} - 3\left(\frac{x_n}{F}\right)^{1/3} + 3\left(\frac{x_x}{F}\right)^{1/3}\right]\right\} .\end{aligned} \tag{13}$$

Evaluating the limits x_x and x_n involves solution of a cubic equation and, referring to Fig. 12, is done as follows. Dropping the subscripts on x, we have

$$R^2 = x^2 + r^2 , \tag{14}$$

$$R^2 = F^2\cos^4\phi = F^2(x/R)^4 . \tag{15}$$

Solving Eq. (15) for R and equating to Eq. (14) we obtain

$$R^6 = (x^2 + r^2)^3 = F^2x^4 \tag{16}$$

or

$$x^2 + r^2 = F^{2/3}x^{4/3} . \tag{17}$$

Setting

$$x = (y + F^{2/3}/3)^{3/2} \tag{18}$$

we find

$$y^3 + \alpha y + \beta = 0 , \tag{19}$$

with $\alpha = -F^{4/3}/3$ and $\beta = r^2 - 2F^2/27$. Solving this cubic in trigonometric form[25] by setting

$$\cos\theta = (-\beta/2)/(-\alpha^3/27)^{1/2} = (1 - 27r^2/2F^2) \tag{20}$$

and returning to variable x, we obtain as limits

$$x_x = F(\tfrac{2}{3}\cos\tfrac{1}{3}\theta + \tfrac{1}{3})^{3/2} \tag{21}$$

and

$$x_n = F[\tfrac{2}{3}\cos(\tfrac{1}{3}\theta + \tfrac{4}{3}\pi) + \tfrac{1}{3}]^{3/2} . \tag{22}$$

The number of incident electrons I penetrating the disk beyond radius r is then

$$\begin{aligned}I = N_e\Sigma = \tfrac{1}{4}N_e\pi b^2F[(r^2/F^2)(U^{-3/2} - V^{-3/2}) + V^{3/2} \\ - U^{3/2} - 3V^{1/2} + 3U^{1/2}] ,\end{aligned} \tag{23}$$

where N_e is number of "free" electrons per cubic centimeter,[6]

$$U = \tfrac{2}{3}\cos[\tfrac{1}{3}\arccos(1 - 27r^2/2F^2)] + \tfrac{1}{3} , \tag{24}$$

$$V = \tfrac{2}{3}\cos[\tfrac{1}{3}\arccos(1 - 27r^2/2F^2) + \tfrac{4}{3}\pi] + \tfrac{1}{3} , \tag{25}$$

and other terms have been previously defined. In

the absence of saturation and/or quenching effects, we should expect I[Eq. (23)] to be proportional to luminescence according to Eq. (1).

4. Number density

In order to evaluate these saturation effects we need to develop a density profile $\rho(r)$ of the number of electrons penetrating a unit area of the disk at radius r. This "areal" number density $\rho(r)$ is obtained by differentiating Eq. (23) with respect to area dA:

$$\rho(r) = \frac{-dI}{dA} = \frac{-dI}{2\pi r dr}$$
$$= \frac{-N_e b^2 F}{8r}\left[\frac{2r}{F^2}(U^{-3/2} - V^{-3/2}) + \frac{3}{2}\frac{r^2}{F^2}\left(V^{-5/2}\frac{dV}{dr} - U^{-5/2}\frac{dU}{dr}\right) + \frac{3}{2}(V^{1/2} - V^{-1/2})\frac{dV}{dr} - \frac{3}{2}(U^{1/2} - U^{-1/2})\frac{dU}{dr}\right], \quad (26)$$

where

$$\frac{dU}{dr} = \frac{-2\sin[\frac{1}{3}\arccos(1 - \frac{27}{2}r^2/F^2)]}{F(3 - \frac{81}{4}r^2/F^2)^{1/2}} \quad (27)$$

and

$$\frac{dV}{dr} = \frac{-2\sin[\frac{1}{3}\arccos(1 - \frac{27}{2}r^2/F^2) + \frac{4}{3}\pi]}{F(3 - \frac{81}{4}r^2/F^2)^{1/2}} . \quad (28)$$

5. Boundary conditions on r

It is instructive to examine the extreme values of r bounding I [Eq. (23)] and/or $\rho(r)$ [Eq. (26)].

a. Small r. On reexamination of Fig. 12, it becomes apparent that we have neglected the impact parameter p (separation of the electron from the initial path of the heavy ion) with respect to the value of r. As r approaches zero, it is clear that its minimum value should not be less than the impact parameter[23] as given by

$$p = (b/2)\tan\phi . \quad (29)$$

A ball-park estimate of the minimum value of r (for which our model is valid) may be made by calculating that impact parameter which gives rise to a 62-eV scattered electron. This latter energy represents the average binding energy of an electron in NE-102,[6] and corresponds to the maximum separation (from the heavy-ion-trajectory axis) for which the electron may still be ejected from its bound condition. By use of Eqs. (3), (5), and (29) and with a suitable choice of terms ($E_1/M_1 = 1$ MeV/nucleon, $Z_1 = 10$), we arrive at a value of about 1 Å for the impact parameter. Such distances, as we shall see in Sec. III B 6 b, are small compared to the radial dimensions of the cylinder defined by the maximum radial range of the scattered electrons. We are assured then that the present model [Eqs. (23) and (26)] is reasonably accurate at distances beyond about 1 Å from the heavy-ion trajectory. Moreover, since we will see below that saturation effects extend well beyond these small radial distances, a detailed picture within this distance is not needed at present.

b. Large r. The largest value of r is defined by the maximum-range projection along the radial axis. Referring again to Fig. 12, we can find this maximum radial distance by finding the maximum in the curve of Eq. (7), viz., $R = F\cos^2\phi$.

Recognizing that $r = R\sin\phi$, we obtain

$$r = F\cos^2\phi\sin\phi . \quad (30)$$

Differentiating r with respect to ϕ and setting the result equal to zero, the conditions for a maximum, we obtain

$$r_{max} = 2F/3\sqrt{3} . \quad (31)$$

6. Number-density profiles

a. Application to heavy ions. In order to make the model applicable to heavy ions, Eq. (3) is simply modified by replacing Z with the effective-ion charge Z_{eff} as suggested by Barkas,[18]

$$Z_{eff} = Z_1(1 - e^{-125\beta Z_1^{-2/3}}) , \quad (32)$$

where $\beta = V_1/c$, c being the velocity of light in vacuum.

b. Constant-velocity profiles. Examples of num-

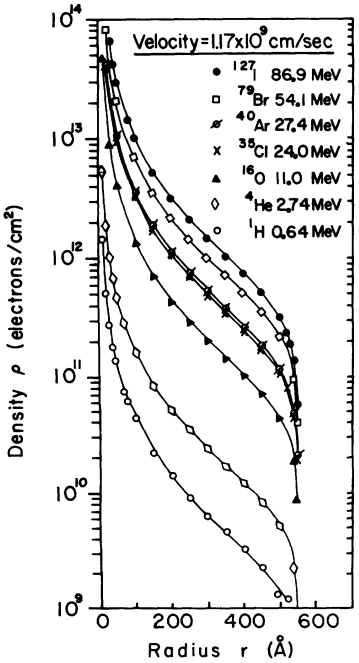

FIG. 13. Areal number density of scattered electrons vs distance r from trajectory axis of indicated heavy ions of velocity 1.17×10^9 cm/sec.

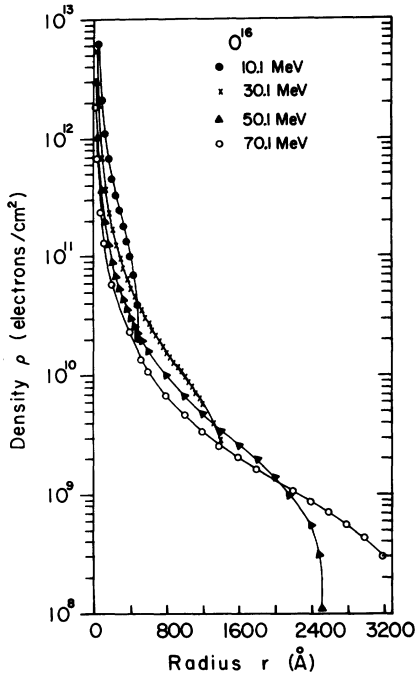

FIG. 14. Areal number density of scattered electrons vs distance from trajectory axis for ^{16}O ions of various energies.

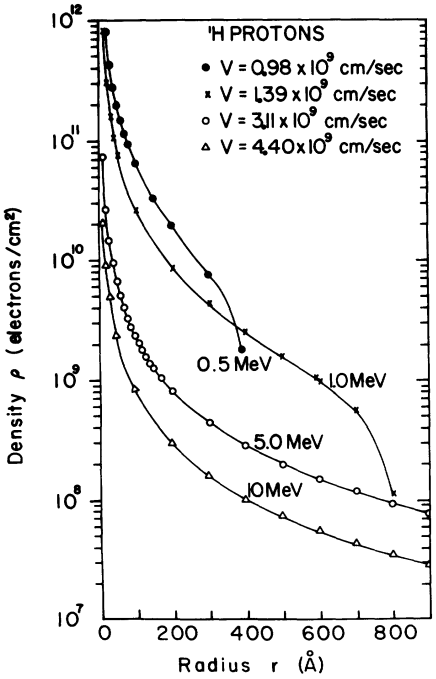

FIG. 16. Areal number density of scattered electrons vs distance from trajectory axis for protons of various energies. This plot is used to infer range of values appropriate to parameter ρ_c for which saturation of luminescence centers is proposed to occur.

ber-density profiles for selected ions of given velocity are shown in Fig. 13. The profiles (log scale) are characterized by large values at small r, a "shoulder" in the middle-r range and a zero value at r_{max}. The shoulder is most pronounced for higher-Z ions.

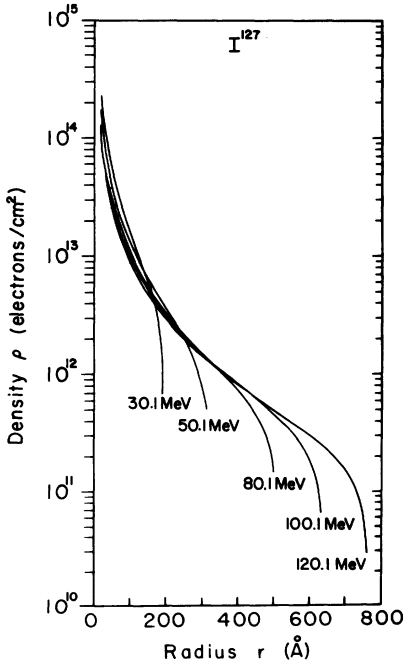

FIG. 15. Areal number density of scattered electrons vs distance from trajectory axis for ^{127}I ions of various energies.

c. Constant-Z profiles. For a given ion, number-density profiles at different ion energies are shown in Figs. 14 and 15 for ^{16}O and ^{127}I ions, respectively. Briefly, we see that near small r the number density *increases* with lower velocities; this trend is reversed at larger values of r. The shoulder is more evident at higher velocity.

d. Saturation level. We introduce the concept of saturation of luminescence centers by supposing that there exists some critical value of number density ρ_c above which all luminescence centers (in the volume element of interest) are excited. Below this value, the number of luminescence centers excited per volume is proportional to number density. Although this formulation produces an unrealistic sharp cutoff in the dependence of excited luminescence centers vs $\rho(r)$ it will suffice for the present development. Accordingly, for a given ion of particular velocity, there exists a saturation radius r_{sat} for which number density is equal to ρ_c. Within the cylindrical volume defined by r_{sat}, the luminescence (per heavy-ion path length) production is taken as proportional to the product $\rho_c \pi r_{sat}^2$. Beyond r_{sat}, the number of luminescence centers excited per unit volume is pro-

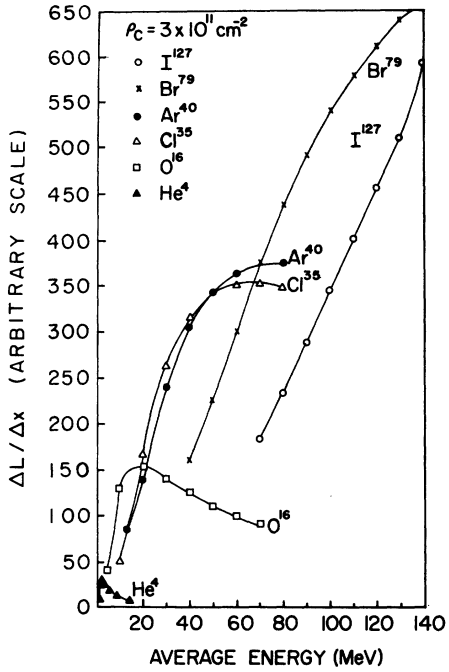

FIG. 17. Calculated specific luminescence vs average ion energy for various heavy ions using $\rho_c = 3 \times 10^{11}$ cm^{-2}. This figure is to be compared with experimental plot of Fig. 11.

portional to $\rho(r)$.

The parameter ρ_c is the only parameter in this model with some degree of choice. The range of values allowed is not altogether unlimited, however. We know, for example, that protons exhibit a fairly linear specific-luminescence-response dependence on specific energy loss above about 5–10-MeV energy. This fact requires that the value of ρ_c be somewhere above the typical value of $\rho(r)$ at small r for 5–10-MeV protons. Figure 16 suggests a range of ρ_c values from 10^{11} to 10^{12} cm^{-2}, for which a significant portion of the projected radial range r has $\rho(r)$ exceeding ρ_c.

7. *Specific luminescence*

We now assign a thickness δx to our thin disk from which the element of differential luminescence δL is produced. The luminescence response will be the sum of the saturated luminescence output from within the cylindrical volume defined by πr_{sat}^2 and the luminescence generated in the cylindrical sleeve bounded by r_{sat} and r_{max}. The latter luminescence value is taken as proportional to the integral

$$\int_{r_{\text{sat}}}^{r_{\text{max}}} \rho(r) 2\pi r \, dr = I(r_{\text{sat}}) \tag{33}$$

under the assumption that $\sigma(E)$ is constant [see Eq. (1)].

This constant σ and n, the number of scintillator sites per unit volume, are included in the constant of proportionality. Further, we have simplified the picture by considering the incident electrons as passing perpendicularly through the plane of the disk when in fact the angle of passage ranges from ϕ_n to ϕ_x [see Eqs. (10) and (11)]. This approximation is least harmful at larger values of r, for which the range in ϕ is more narrow. At smaller values of r, the effect of a wider range in ϕ is partially covered by the saturation effects previously mentioned. Thus the relation for specific luminescence in the thin disk is given as

$$\frac{\delta L}{\delta x} \approx \pi r_{\text{sat}}^2 \rho_c + I(r_{\text{sat}}) \, . \tag{34}$$

Since the thin film may be considered to be composed of a large number of these planes of thickness δx, the specific luminescence of the thin film, $\Delta L/\Delta x$, is taken as the sum of $\delta L/\delta x$ from each individual disk. We neglect "end" effects appearing in the vicinity of the heavy-ion entrance and exit points of the thin film. Finally, therefore, we have

$$\frac{\Delta L}{\Delta x} = C[\pi r_{\text{sat}}^2 \rho_c + I(r_{\text{sat}})] \, , \tag{35}$$

with $C = \sigma n$ accepted as constant.

Examples of specific luminescence calculated in this manner are shown as a function of ion energy in Fig. 17 for a value of ρ_c equal to 3×10^{11} electrons/cm^2. In view of the wide ranges of energies and the wide variety of ions considered, and in view of the unrefined nature of the present model, the over-all agreement with experiment (compare with Fig. 11) is quite satisfying. A comprehensive discussion of the details of this model will be rendered in a future work.

IV. SUMMARY

The thin-film scintillator detector is a unique tool for measuring *directly* relative specific-luminescence ($\Delta L/\Delta x$) and luminescence-efficiency ($\Delta L/\Delta E$) values of organic scintillators. These experimentally obtained luminescence data are presented as a function of ion energy, velocity, and stopping power for a wide variety of transiting ions ($Z = 1, 2, 8, 17, 18, 35, 53$). The data emphasize the luminescence response in the low-energy range corresponding to maximum ion stopping power. Common trends, unique characteristics, and other interesting features pertinent to these graphical plots are noted and discussed.

The double-valuedness of the specific luminescence, $\Delta L/\Delta x$, when plotted as a function of specific energy loss, $\Delta E/\Delta x$, is interpreted as arising mainly from the decreased effective charge of the ion as it picks up electrons in the slowing-down process. It is further emphasized that the specific

energy loss *per se* is an inappropriate parameter for characterizing (in a direct way) the luminescence response in this lower-energy region.

A new model is formulated based on a conceptually different approach to the problem of luminescence production along and about the path of a transiting energetic ion. In essence, the number of electrons scattered into a thin disk of scintillator material (perpendicular to the ion trajectory) is taken, in the absence of saturation effects, as proportional to the luminescence response from that disk. Saturation effects are included by deriving an explicit relation for the number of electrons scattered per unit area of disk at a distance r from the ion path. Above a critical number per unit area, no additional luminescence response is generated. These number-density profiles are plotted for various ions of different energies. Finally, a plot of the calculated specific luminescence for various heavy ions is shown to be in remarkably good agreement with experimental data.

ACKNOWLEDGMENTS

The assistance of Professor H. Weller, Department of Physics, throughout the use of the University of Florida Van de Graaff accelerator is much appreciated. We are indebted to the staff and personnel of the Florida State University tandem Van de Graaff facility for the cooperation leading to the ^{16}O experiments. In particular, our thanks to Professor H. Plendl, Physics Department, F. S. U., for his aid. For the heavy-ion data, we express our thanks to G. F. Wells and the staff of the ORNL tandem Van de Graaff accelerator for their cooperation. Computer analysis of the luminescence model described herein was performed at and partially funded by the North East Regional Data Center, University of Florida.

---

*Supported in part by the U. S. Atomic Energy Commission through contract AT (40-1) 2843.

[1]J. B. Birks, Proc. Phys. Soc., Lond. A 63, 1294 (1950); Phys. Rev. 84, 364 (1951); 86, 569 (1952); J. W. King and J. B. Birks, Phys. Rev. 86, 568 (1952).

[2]W. K. Jentschke, F. S. Eby, C. J. Taylor, M. E. Remley, and P. G. Kruger, Phys. Rev. 83, 170 (1951); 84, 1034 (1951).

[3]S. K. Allison and H. Casson, Phys. Rev. 90, 880 (1955).

[4]C. B. Fulmer, Phys. Rev. 108, 1113 (1957).

[5]E. Newman and F. E. Steigert, Phys. Rev. 118, 1575 (1960); A. M. Smith, Phys. Rev. 122, 1520 (1961).

[6]R. Voltz, J. Lopes da Silva, G. Laustriat, and A. Coche, J. Chem. Phys. 45, 3306 (1966).

[7]M. R. Altman, H. B. Dietrich, and R. B. Murray, Phys. Lett. A 32, 423 (1970).

[8]J. Lopes da Silva and R. Voltz, Rev. Phys. Appl. 7, 127 (1972).

[9]M. L. Muga, Nucl. Instrum. Methods 95, 349 (1970); M. L. Muga, D. J. Burnsed, and W. E. Steeger, Nucl. Instrum. Methods 104, 605 (1972).

[10]L. Muga and G. Griffith, Nucl. Instrum. Methods 109, 289 (1973).

[11]L. Muga and G. Griffith, Phys. Rev. B 8, 4069 (1973).

[12]L. Muga, G. Griffith, H. Schmitt, and H. Taylor, Nucl. Instrum. Methods 111, 581 (1973).

[13]Obtainable from Nuclear Enterprises, Inc., San Carlos, Calif.

[14]R. B. Murray and A. Meyer, Phys. Rev. 122, 815 (1961).

[15]M. Luntz and G. Heymsfield, Phys. Rev. B 6, 2530 (1972).

[16]R. Katz and E. J. Kobetich, Phys. Rev. 170, 397 (1968).

[17]L. C. Northcliffe and R. F. Schilling, Nucl. Data A 7, 233 (1970).

[18]W. H. Barkas, *Nuclear Research Emulsions* (Academic, New York, 1963), Vol. 1, p. 371.

[19]A. Meyer and R. B. Murray, Phys. Rev. 128, 98 (1962).

[20]E. J. Kobetich and R. Katz, Phys. Rev. 170, 391 (1968).

[21]M. Luntz, Phys. Rev. B 4, 2857 (1971).

[22]G. Friedlander, J. W. Kennedy, J. M. Miller, *Nuclear and Radio-Chemistry*, 2nd ed. (Wiley, New York, 1964), p. 63.

[23]R. D. Evans, *The Atomic Nucleus* (McGraw-Hill, New York, 1955), pp. 828–851.

[24]K. H. Weber, Nucl. Instrum. Methods 25, 261 (1964).

[25]*Handbook of Mathematical Tables*, 1st ed., edited by G. D. Hodgman (Chemical Rubber, Cleveland, Ohio, 1962), pp. 387, 388.